Inorg. Chem. **2006**, *45*, 10595–10604

Donor–Acceptor Interactions and Electron Transfer in Cyano-Bridged Trinuclear Compounds

Pablo Alborés, Melina B. Rossi, Luis M. Baraldo, and Leonardo D. Slep*

Departamento de Química Inorgánica, Analítica y Química Física, INQUIMAE, Facultad de Ciencias Exactas y Naturales Universidad de Buenos Aires, Pabellón 2, Ciudad Universitaria, C1428EHA Buenos Aires, Argentina

Received June 30, 2006

The NIR donor–acceptor charge transfer (DACT) bands of the series of trinuclear complexes *trans*-$[(NC)_5Fe^{II/III}$-$(\mu$-$CN)Ru^{II}L_4(\mu$-$NC)Fe^{III}(CN)_5]^{5/4-}$ (L= pyridine, 4-*tert*-butylpyridine, and 4-methoxypyridine) are analyzed in terms of a simplified molecular orbital picture that reflects the interaction between the donor and acceptor fragments. The degree of electronic coupling between the fragments is estimated by a full fit of the DACT band profiles according to a three-state model inspired in the Mulliken–Hush formalism. The information is complemented with determinations performed on the asymmetric heterotrinuclear species *trans*-$[(NC)_5Co^{III}(\mu$-$CN)Ru^{II}(py)_4(\mu$-$NC)Fe^{III}(CN)_5]^{4-}$, whose preparation is reported here for the first time. The analysis of the NIR spectra of the symmetric *trans*-$[(NC)_5Fe^{III}$-$(\mu$-$CN)Ru^{II}L_4(\mu$-$NC)Fe^{III}(CN)_5]^{4-}$ species reveals a low degree of mixing between the terminal acceptor fragments and the bridging moiety containing Ru^{II}, with H_{12} values between1.0×10^3 and 1.5×10^3 cm^{-1}. The reorganization energy contributions seem to be the same for the three species, even when the spectra were recorded in different media. This observation also applies for the Co^{III}-substituted compound. The computed potential energy surfaces (PES) of the ground state for these complexes show only one stationary point, suggesting that the Fe^{II}–Ru^{III}–Fe^{III} (or Fe^{II}–Ru^{III}–Co^{III}) electronic isomers are not thermally accessible. One-electron reduction leads to asymmetric *trans*-$[(NC)_5Fe^{II}(\mu$-$CN)Ru^{II}L_4(\mu$-$NC)Fe^{III}(CN)_5]^{5-}$ compounds with potentially two DACT bands involving the Ru^{II} and the Fe^{II} donor fragments. These species reveal a similar degree of electronic mixing but the PES shows three minima. We explore the role of the bridging fragment in the long-range thermally induced electron transfer between the distant iron centers. The results suggest that superexchange and hopping might become competitive paths, depending on the substituents in the bridging fragment.

Introduction

Over the past decades, the thermally induced electron-transfer process between donor−acceptor (D−A) dyads and its connection to the donor−acceptor charge transfer (DACT) spectroscopy has been extensively studied.[1] Pioneering work linked the oscillator strength of the DACT with the D−A electronic coupling at the ground-state equilibrium geometry of weakly coupled D−A pairs and led to the well-established Hush formalism,[2] which relies on the Born−Oppenheimer approximation and first-order perturbation theory arguments. The D−A interaction is described in terms of the electronic coupling element, H_{DA}, which can be estimated from the extinction coefficient (ϵ_{max} in M^{-1} cm^{-1}), the full width at half-height ($\Delta\nu_{1/2}$ in cm^{-1}), the maximum wavenumber (ν_{max} in cm^{-1}), and the transition dipole length (r_{DA} in Å) of the experimental DACT band, whose band-shape is assumed to be Gaussian

$$H_{DA} = (0.0205/r_{DA})[\epsilon_{max}\Delta\nu_{1/2}\nu_{max}]^{1/2} \quad (1)$$

This level of analysis has proved to be successful for the elucidation of the electronic properties of many mixed-valent species, particularly those containing redox-active transition metal ions.[2c−d]

The field experienced a renaissance because of recent synthetic achievements, which yielded D−A systems of

* To whom correspondence should be addressed. E-mail: slep@qi.fcen.uba.ar.

(1) (a) Newton, M. D. *Chem. Rev.* **1991**, *91*, 767−792. (b) Balzani, V. *Electron Transfer in Chemistry*; Wiley-VCH: Weinheim, Germany, 2001; Vol. 1.

(2) (a) Marcus, R. A.; Sutin, N. *Biochim. Biophys. Acta* **1985**, *811*, 265. (b) Hush, N. S. *Prog. Inorg. Chem.* **1967**, *8*, 391. (c) Brunschwig, B. S.; Creutz, C.; Sutin, N. *Coord. Chem. Rev.* **1998**, *177*, 61−79. (d) Creutz, C. *Prog. Inorg. Chem.* **1983**, *30*, 1−73.

10.1021/ic061202k CCC: $33.50
Published on Web 11/18/2006

higher complexity, such as donor−bridge−acceptor (D−B−A) triads based on purely organic redox-active fragments linked by an unsaturated π-bridge,[3,4] bimetallic coordination compounds linked by redox active organic molecules,[5] and others. These new compounds resulted in a rich debate concerning the role played by the bridging fragment in the mechanism of electron transfer in covalently linked donor−acceptor systems because the bridge moiety B can be intimately involved in the electron-transfer process behaving as a D or A component.

In some selected cases, the timescale for the interconversion between electronic isomers provided a deeper insight into the electron-transfer mechanisms.[6] This is not always the case, and electronic spectroscopy is still the method of choice in most of the situations. The realization that a great deal of information concerning the D−A electronic coupling is contained in the spectral band-shape, which can be far from Gaussian, led to more sophisticated treatments[7] that were employed with relative success to extract information from the DACT spectra of complex systems.

We have recently reported the synthesis, characterization, and spectroscopic properties of a family of trinuclear cyano-bridged mixed-valent compounds *trans*-$[(NC)_5Fe^{III}(\mu\text{-}CN)Ru^{II}L_4(\mu\text{-}NC)Fe^{III}(CN)_5]^{4-}$, with L = pyridine (**1**), 4-*tert*-butylpyridine (**2**), and 4-methoxypyridine (**3**), that seem to be good candidates to begin a systematic investigation on the mechanisms involved in electron-transfer events between metallic fragments.[8] These compounds reveal intense bands ($\epsilon \approx 2000-9000\ M^{-1}\ cm^{-1}$) in the NIR region of the spectrum, which are not present in any of the constituting fragments. These intervalence DACT bands seem to originate in metal-to-metal charge-transfer transitions from the bridging Ru(II) fragment to the terminal Fe(III) moieties and show the electronic coupling in these A−D−A systems. The IV (or DACT) bands are slightly asymmetric, with noticeable tails to the high-energy side of the spectrum. The very same band-shape, though less intense, is observed for the (IV) CT band of the complex *trans*-$[(NC)_5Fe^{III}(\mu\text{-}CN)Ru^{II}(py)_4(\mu\text{-}NC)Co^{III}(CN)_5]^{4-}$ (**4**), reported here for the first time and designed deliberately as a dinuclear model for the symmetric trinuclear complexes **1**−**3**.

In our previous work, we also showed that these molecules are redox active. The one-electron-reduced mixed-valent $\{Fe^{II}-Ru^{II}-Fe^{III}\}$ systems exhibit intense red-shifted bands in the NIR region of the spectrum. These species appear to behave as D−D−A systems, and the NIR transitions probably involve the superposition of a MMCT band from the central Ru^{II} to the terminal Fe^{III} fragments and an $Fe^{II} \rightarrow Fe^{III}$ long-range CT transition.

We report here on our implementation of the generalized Mulliken−Hush theory for these trinuclear systems, and our findings on the analysis of their electronic spectra. The treatment leads to a description of the ground state's potential energy surface (PES) and therefore is relevant to understanding the electron-transfer processes between the terminal fragments.

Experimental Section

Materials. The compound $[Ru(py)_5Cl](PF_6)$ was synthesized according to literature procedures.[9] Tetra-*n*-butylammonium hexafluorophosphate, $TBAPF_6$, was recrystallized from ethanol. Solvents for UV−vis−NIR spectroscopy and electrochemistry measurements were dried according to literature procedures.[10] All other reagents were obtained commercially and used as supplied. All the symmetric trinuclear complexes and their reduced species were available from a previous work.[8]

Preparation of *trans*-$[(NC)_5Fe^{III}(\mu\text{-}CN)Ru^{II}(py)_5](Ph_4P)\cdot 6H_2O$. $[Ru(py)_5Cl](PF_6)$ (300 mg) was suspended in 50 mL of methanol and treated with a solution of 175 mg of $K_3Fe(CN)_6\cdot 3H_2O$ in 50 mL of water. The resulting mixture was stirred at 40 °C in the dark for about 5 h. After this period, the resulting green solution was filtered to remove a small amount of unreacted ruthenium precursor and then evaporated to dryness. The solid residue was extracted with methanol to eliminate the excess of potassium ferricyanide, and the clear green solution was evaporated to dryness. The green solid was dissolved in a minimum amount of water and treated with solid tetraphenylphosphonium chloride (Ph_4PCl). The pale green precipitate was collected by filtration, washed several times with water, and vacuum-dried. The crude solid was dissolved in a minimum amount of methanol, and after filtration, the green solution was loaded in a Sephadex LH-20 column packed with methanol. The second green fraction that eluted with methanol contained the desired product, which was collected and evaporated to dryness to yield 174 mg (34%). Anal. Calcd for $C_{55}H_{57}N_{11}O_6PFeRu$: C, 57.1; H, 4.9; N, 13.3. Found: C, 56.8; H, 4.6; N, 13.8. ν(CN): 2109 cm^{-1}(s).

Preparation of *trans*-$[(NC)_5Fe^{III}(\mu\text{-}CN)Ru^{II}Py_4(\mu\text{-}NC)Co^{III}(CN)_5](Ph_4P)_4\cdot 9H_2O$ (4). *trans*-$[(NC)_5Fe^{III}(\mu\text{-}CN)Ru^{II}(py)_5](Ph_4P)\cdot 6H_2O$ (200 mg) was dissolved in 30 mL of methanol and was treated with a solution of 630 mg of $K_3Co(CN)_6$ in 30 mL of water. The green solution was stirred at 65 °C in the dark for 3 h. After this period the solvent was evaporated, leaving a solid residue that was extracted with methanol to remove the insoluble excess of potassium cobalticyanide. The methanolic green solution was evaporated to dryness, and the solid redissolved in a minimum amount of water.

(3) (a) Lambert, C.; Noll, G. *Angew. Chem., Int. Ed.* **1998**, *37*, 2107−2110. (b) Lambert, C.; Noll, G. *J. Am. Chem. Soc.* **1999**, *121*, 8434−8442. (c) Lambert, C.; Noll, G. *J. Chem. Soc., Perkin Trans. 2* **2002**, 2039−2043.

(4) Lambert, C.; Noll, G.; Schelter, J. *Nat. Mater.* **2002**, *1*, 69−73.

(5) (a) Evans, C. E. B.; Naklicki, M. L.; Rezvani, A. R.; White, C. A.; Kondratiev, V. V.; Crutchley, R. J. *J. Am. Chem. Soc.* **1998**, *120*, 13096−13103. (b) Evans, C. E. B.; Yap, G. P. A.; Crutchley, R. J. *Inorg. Chem.* **1998**, *37*, 6161−6167. (c) Mosher, P. J.; Yap, G. P. A.; Crutchley, R. J. *Inorg. Chem.* **2001**, *40*, 1189−1195. (d) Crutchley, R. J. *Coord. Chem. Rev.* **2001**, *219*, 125−155. (e) Kar, S.; Sarkar, B.; Ghumaan, S.; Janardanan, D.; van Slageren, J.; Fiedler, J.; Puranik, V. G.; Sunoj, R. B.; Kaim, W.; Lahiri, G. K. *Chem.—Eur. J.* **2005**, *11*, 4901−4911.

(6) (a) Londergan, C. H.; Salsman, J. C.; Lear, B. J.; Kubiak, C. P. *Chem. Phys.* **2006**, *324*, 57−62. (b) Salsman, J. C.; Kubiak, C. P. *J. Am. Chem. Soc.* **2005**, *127*, 2382−2383. (c) Salsman, J. C.; Ronco, S.; Londergan, C. H.; Kubiak, C. P. *Inorg. Chem.* **2006**, *45*, 547−554.

(7) (a) Brunschwig, B. S.; Creutz, C.; Sutin, N. *Chem. Soc. Rev.* **2002**, *31*, 168−184. (b) Lockard, J. V.; Valverde, G.; Neuhauser, D.; Zink, J. I.; Luo, Y.; Weaver, M. N.; Nelsen, S. F. *J. Phys. Chem. A* **2006**, *110*, 57−66. (c) Talaga, D. S.; Zink, J. I. *J. Phys. Chem. A* **2001**, *105*, 10511−10519. (d) Ferretti, A.; Lami, A. *Chem. Phys. Lett.* **1994**, *220*, 327−330. (e) Ondrechen, M. J.; Ferretti, A.; Lami, A.; Villani, G. *J. Phys. Chem.* **1994**, *98*, 11230−11232.

(8) Albores, P.; Slep, L. D.; Weyhermuller, T.; Baraldo, L. M. *Inorg. Chem.* **2004**, *43*, 6762−6773.

(9) Coe, B. J.; Meyer, T. J.; White, P. S. *Inorg. Chem.* **1995**, *34*, 593−602.

(10) Armarego, W. L. F.; Perrin, D. D. *Purification of Laboratory Chemicals*, 4th ed.; Butterworth-Heinemann: Oxford, U.K., 1996.

Solid Ph_4PCl was added to this solution, and the solid obtained was filtered and washed with water. The crude product was dissolved in a minimum amount of methanol, filtered, and loaded into a methanol-packed Sephadex LH-20 column. The product eluted with methanol as the first green fraction. Evaporation to dryness and recrystallization from methanol/ether afforded 70 mg (16%) of the final product. Anal. Calcd for $C_{128}H_{118}N_{16}O_9P_4FeCoRu$ **(4)**: C, 65.0; H, 5.0; N, 9.5; Found: C, 64.7; H, 5.5; N, 10.0. ν(CN): 2120 cm^{-1}(s), 2107 cm^{-1}(s).

Physical Measurements. IR spectra were collected with a Nicolet FTIR 510P instrument on KBr pellets. UV−vis−NIR spectra were recorded with a Shimadzu 3100 double-beam spectrophotometer (up to 3000 nm). Elemental analyses were performed with a Carlo Erba 1108 analyzer. Cyclic voltammetry measurements were carried out under argon with millimolar solutions of the compounds using a PAR 273A potentiostat and a standard three-electrode arrangement consisting of a glassy carbon disk (ϕ = 3 mm) as the working electrode, a platinum wire as the counter electrode, and a reference electrode. The latter was either a Ag/AgCl (KCl 3 M) standard electrode (for aqueous solutions) or a silver wire with an internal ferrocene (Fc) standard for organic solvents, depending on the situation. KNO_3 (1 M) and $TBAPF_6$ (0.1 M) were used as the supporting electrolytes in water and nonaqueous media, respectively. All the potentials reported in this work are referenced to the standard Ag/AgCl (KCl 3 M) electrode (0.21 V vs NHE), with the conversions being performed by using the accepted values for the Fc^+/Fc couple in different media (195 ± 4, 418 ± 2, 479 ± 2, 507 ± 2, and 582 ± 7 mV vs Ag/AgCl (KCl 3 M) for water, methanol, ethanol, acetonitrile, and dimethylacetamide, respectively).[11]

Results and Discussion

Synthesis and Characterization of *trans*-$[(NC)_5Fe^{III}(\mu\text{-}CN)Ru^{II}(py)_4(\mu\text{-}NC)Co^{III}(CN)_5](Ph_4P)_4\cdot 9H_2O$. The differential reactivity of the axial ligands of $[Ru(py)_5Cl]^+$ against substitution by hexacyanoferrate(III) is the key factor in the synthesis of asymmetric compound **4**. This species can be prepared and isolated in good yield if the stoichiometry and temperature of the synthetic steps are kept under control. At T < 40 °C with $[Ru(py)_5Cl]^+$ and $[Fe(CN)_6]^{3-}$ in a 1:1 ratio, the main product is the dinuclear *trans*-$[(NC)_5Fe^{III}(\mu\text{-}CN)\text{-}Ru^{II}(py)_5]^-$ with only marginal amounts of *trans*-$[(NC)_5Fe^{III}\text{-}(\mu\text{-}CN)Ru^{II}(py)_4(\mu\text{-}NC)Fe^{III}(NC)_5]^{4-}$ (**1**) as the main contaminant. The reaction of this intermediate species with an excess of hexacyanocobaltate(III) under mild conditions, followed by size exclusion chromatography affords the asymmetric trinuclear species *trans*-$[(NC)_5Fe^{III}(\mu\text{-}CN)Ru^{II}\text{-}(py)_4(\mu\text{-}NC)Co^{III}(CN)_5]^{4-}$.

Compounds **1** and **4** are formally related by a substitution of one Fe^{III} ion by a Co^{III} ion. We carried out this exchange procedure to facilitate the analysis of the electronic interactions that are present in an A−D−A ensemble. In this system, only one D−A interaction is relevant to the electronic spectroscopy. The electrochemistry and electronic spectroscopy of **4** suggest that the Fe^{III}−Co^{III} exchange did not perturb the D−A interaction between the remaining redox-active fragments. In fact, the cyclic voltammogram of **4** compares well with the one of the related symmetric complex **1**. Two reversible waves are observed in the cyclic voltammetry measurements which are attributed to the Ru^{III}/Ru^{II} and Fe^{III}/Fe^{II} redox processes (inset of Figure 1). The lack of the second Fe^{III}/Fe^{II} process and the existence of an irreversible reduction process corresponding to the Co^{III}/Co^{II} couple are compatible with the formulation of complex **4**. This last irreversible redox process closely resembles the behavior of free $[Co(CN)_6]^{3-}$.

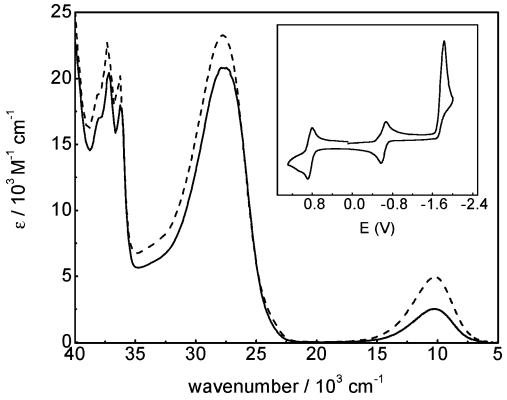

Figure 1. Electronic spectrum of compounds **1** (dashed line) and **4** (solid line) in methanol. The inset shows the cyclic voltammogram of compound **4** in acetonitrile/0.1 M $TBAPF_6$. Scan rate = 100 mV s^{-1}. The potentials referred to the standard Ag/AgCl (KCl 3 M) electrode.

Table 1. Spectroscopic Data for Compound **4**

	MLCT		MM′CT	
solvent	ν_{max} (10^3 cm^{-1})	ϵ (M^{-1} cm^{-1})	ν_{max} (10^3 cm^{-1})	ϵ (M^{-1} cm^{-1})
water	28.7	16 400	7.5	3600
methanol	27.6	20 800	10.2	2500
ethanol	27.1	22 200	10.9	2300
acetonitrile	26.7	19 700	13.3	1300
dimethylacetamide	25.8	23 800	14.3	1100

The UV−vis−NIR spectrum of compound **4** shows the same features as that of complex **1** (Figure 1). It possesses an intense MLCT, $d_\pi(Ru^{II}) \rightarrow \pi^*$(py) band in the UV region and a MM′CT (or DACT) $Ru^{II} \rightarrow Fe^{III}$ band in the near-infrared. The latter is placed at the same energy as the MM′CT band in complex **1** and has the same band shape but only half of the intensity. The solvent dependence of the electronic spectrum of this compound also resembles the behavior of **1** and is related to the CN^-/solvent specific interactions, as discussed elsewhere.[8,12] The spectroscopic data of **4** in different solvents are listed in Table 1.

Theoretical Considerations. We attempt here to improve our understanding of the electronic interactions between the donor and acceptor fragments in the related complexes **1**−**4**. All these species have intense and fairly broad low-energy

(11) Noviandri, I.; Brown, K. N.; Fleming, D. S.; Gulyas, P. T.; Lay, P. A.; Masters, A. F.; Phillips, L. *J. Phys. Chem. B* **1999**, *103*, 6713−6722.

(12) (a) Baraldo, L. M.; Forlano, P.; Parise, A. R.; Slep, L. D.; Olabe, J. A. *Coord. Chem. Rev.* **2001**, *219*, 881−921. (b) Timpson, C. J.; Bignozzi, C. A.; Sullivan, B. P.; Kober, E. M.; Meyer, T. J. *J. Phys. Chem.* **1996**, *100*, 2915−2925. (c) Estrin, D. A.; Baraldo, L. M.; Slep, L. D.; Barja, B. C.; Olabe, J. A.; Paglieri, L.; Corongiu, G. *Inorg. Chem.* **1996**, *35*, 3897−3903. (d) Gonzalez-Lebrero, M. C.; Turjanski, A. G.; Olabe, J. A.; Estrin, D. A. *J. Mol. Model.* **2001**, *7*, 201−206. (e) Hornung, F. M.; Baumann, F.; Kaim, W.; Olabe, J. A.; Slep, L. D.; Fiedler, J. *Inorg. Chem.* **1998**, *37*, 311−316. (f) Ketterle, M.; Kaim, W.; Olabe, J. A.; Parise, A. R.; Fiedler, J. *Inorg. Chim. Acta* **1999**, *291*, 66−73.

Scheme 1. Compounds Studied in This Work

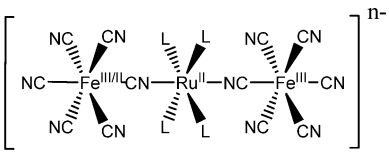

L= pyridine (**1/1r**), 4-*tert*-butylpyridine (**2/2r**) and 4-methoxypyridine (**3/3r**)

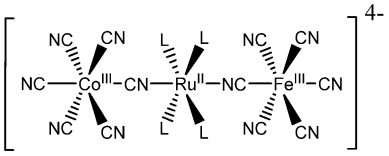

L= pyridine (**4**)

MM′CT (DACT) bands, a fact that has been classically considered to be indicative of moderate/weak electronic coupling between the metal centers. The presence of more than one donor (or acceptor) groups introduces some uncertainty regarding the number and source of the allowed CT transitions. We will first focus on the orbital origin of these transitions and then attempt to obtain quantitative information about the degree of interaction from the absorption profile.

Qualitative Molecular Orbital Interpretation of the MMCT Bands. At the equilibrium geometry, compounds **1**−**3** belong to the D_4 symmetry point group.[8] The t_{2g} sets of each metal center split into $b_2(d_{xy}) + e(d_{xz}, d_{yz})$. The cyanide-mediated overlap between the $e(d_{xz}, d_{yz})$ orbitals of the three metal centers gives rise to the π-backbone represented qualitatively in the MO diagram of Scheme 2. Under D_4 symmetry, there are two dipole allowed transitions, $e_1 \rightarrow e_2$ and $e_1 \rightarrow e_3$, although the former is overlap-forbidden. Nevertheless, this transition might gain intensity upon coupling with an asymmetric vibration mode that lowers the symmetry of the electronic problem to C_4 (Scheme 2). It is tempting to assign the asymmetry of the DACT bands in **1**−**3** to the existence of this second transition. The spectral profile of the DACT band in **4**, identical to that in **1**, shows that this is not necessarily the case. Compound **4** has also C_4 symmetry, but the large energy difference between the Fe^{III} and Co^{III} centered orbitals leads to a situation where only two of the metal centers are involved in the π-backbone. This situation leaves a single observable MMCT transition that is $Ru^{II} \rightarrow Fe^{III}$ ($e_2 \rightarrow e_3$) in origin. Despite this, the shapes (not the intensity) of the NIR region of the spectra of **1** and **4** match perfectly.

The DACT spectroscopy in the one-electron-reduced compounds, **1r**−**3r**, can be analyzed with a similar MO diagram. The asymmetry introduced by the reduction process (Fe^{II} vs Fe^{III}) opens the possibility to two DACT transitions. One of them is $Ru^{II} \rightarrow Fe^{III}$ in character ($e_1 \rightarrow e_3$), and the remaining one is an $Fe^{II} \rightarrow Fe^{III}$ ($e_2 \rightarrow e_3$) CT and is absent in the $Fe^{III}-Ru^{II}-Fe^{III}$ compounds.

The electrochemical results are consistent with this description, and they validate the qualitative MO picture. The redox potential for the first reduction of the Fe^{III} centers remains constant for the different ligands L,[8] indicating that the molecular orbital involved in this process (e_2) has little

Scheme 2. Qualitative MO Diagram Representing the π-Backbone for the Different Situations Studied in This Work[a]

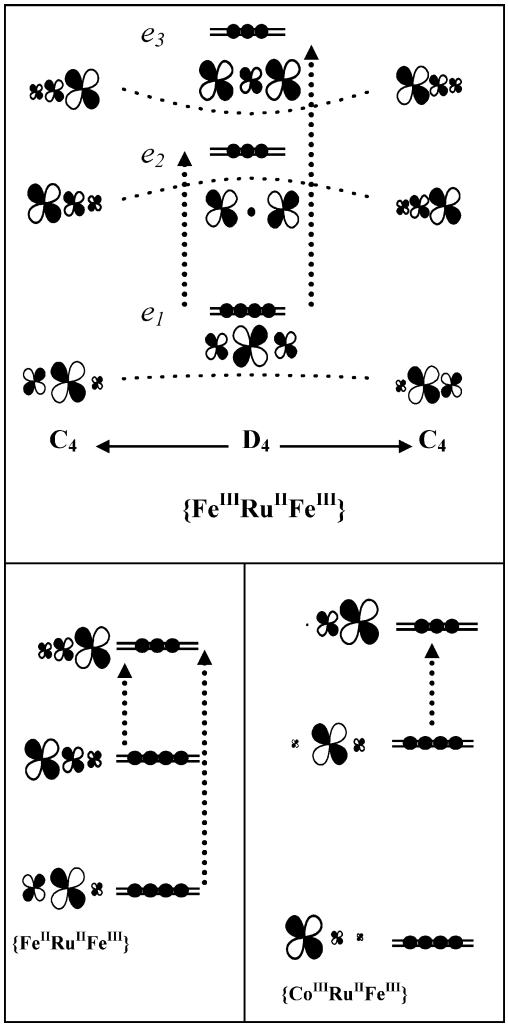

[a] Only one of the components of the doubly degenerate representations is included to facilitate the visualization.

contribution from the Ru^{II} moiety. On the other hand, the redox potential for the second reduction process over the Fe shifts to lower values when the basicity of L is increased, indicating that the molecular orbital involved in this second redox event (e_3) has a considerable Ru^{II} contribution.

No matter how satisfactory this MO scheme is, it does not provide a qualitative explanation concerning the band shape of the DACT bands. Moreover, no quantitative information about the degree of mixing between the metallic moieties can be extracted with this level of analysis. For this reason, the vis−NIR bands of these trinuclear compounds were studied employing tools derived from the generalized Mulliken−Hush (GMH) theory.[13] The absorption profile was simulated with a two-state model in the case of compound **4** and a three-state model for the remaining complexes. The two situations, even though they share essentially the same theoretical background, are slightly different, and we treat them separately for the sake of clarity.

Dinuclear Systems (Two-State Model). This is basically the situation that originated the earliest Mulliken−Hush

(13) Cave, R. J.; Newton, M. D. *Chem. Phys. Lett.* **1996**, *249*, 15−19.

Scheme 3. Diabatic States and Parameter Definitions for a Two-State Model

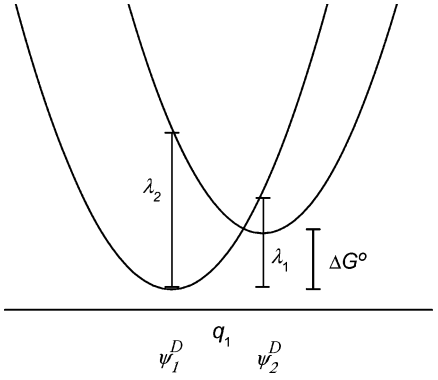

Scheme 4. Diabatic States for a Three-State Model for Compounds **1**−**3** (a) and **1r**−**3r** (b)

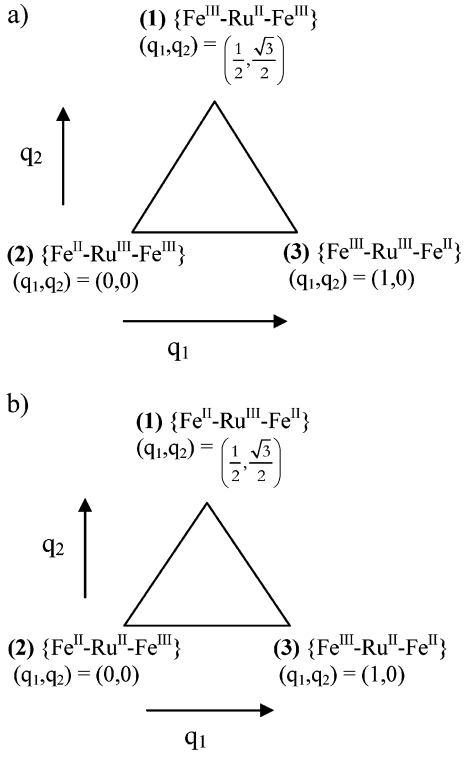

formalism,[2] and our treatment follows basically ref 14. Scheme 3 qualitatively describes the diabatic states and the nonzero matrix elements between them. The problem involves a single dimensionless ET coordinate q_1 that transforms state 1 into state 2, with the two diabatics surfaces approximated as quadratic functions of the ET coordinate. On the basis of the diabatic wave functions, ψ_1^D and ψ_2^D, the Hamiltonian for the system becomes

$$H(q_1) = \begin{pmatrix} \lambda_1 {q_1}^2 & H_{DA} \\ H_{DA} & \Delta G° + \lambda_2 (q_1 - 1)^2 \end{pmatrix} \quad (2)$$

where λ_1 and λ_2 stand for the Marcus reorganization energies associated to the donor and acceptor diabatic states and $\Delta G°$ measures their relative free energies.

(14) Creutz, C.; Newton, M. D.; Sutin, N. *J. Photochem. Photobiol., A* **1994**, *82*, 47−59.

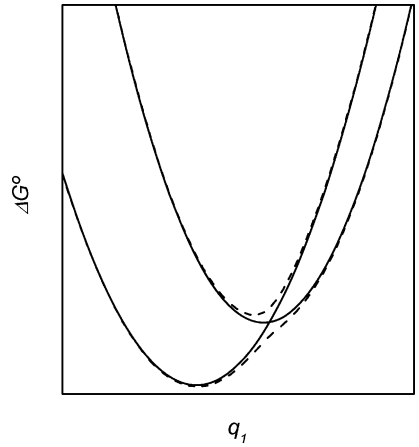

Figure 2. Qualitative diabatic (solid line) and adiabatic (dotted line) potential energy curves for compound **4**.

The electronic interaction represented by the off-diagonal (and coordinate-independent) matrix element H_{DA} leads to mixing of the diabatic surfaces to yield the adiabatic potential energy curves qualitatively depicted in Figure 2. From the mathematical point of view, these curves arise from the diagonalization of eq 2 at each reaction coordinate. This process leads to the ET coordinate-dependent free energies of both states $\Delta G°_1^A(q_1)$ and $\Delta G°_2^A(q_1)$, and the compositions of the adiabatic eigenfunctions in terms of the diabatic state basis set, which satisfy the following relations:

$$\psi_j^A(q_1) = \sum_{i=1}^{2} C_{ij}(q_1)\psi_i^D(q_1) \quad (3)$$

$$\begin{pmatrix} \Delta G°_1^A(q_1) & 0 \\ 0 & \Delta G°_2^A(q_1) \end{pmatrix} = C(q_1)^{-1} \times H(q_1) \times C(q_1) \quad (4)$$

The same unitary transformation that diagonalizes the Hamiltonian brings the transition moment matrix from the diabatic into the adiabatic representation (eq 5)

$$\mu^A(q_1) = C(q_1)^{-1} \times \mu^D \times C(q_1) \quad (5)$$

After the treatment by Cave and Newton,[13] μ^D was taken as

$$\mu^D = \begin{pmatrix} 0 & 0 \\ 0 & er_{12} \end{pmatrix} \quad (6)$$

where the transition moments connecting the diabatic states were set to zero[13,14] and er_{12} is the difference between the dipole moments of the initial and final diabatic (localized) states.

From a semiclassical point of view, the differential contribution to the absorption spectrum arising from a specific nuclear configuration, q_1, belonging to the ground adiabatic state energy surface is given by

$$d\epsilon(n) = \frac{4\pi^2 \nu}{3\hbar c n_t} |\mu_{12}^A(q_1)|^2 \, \delta(\nu - (\Delta G°_2^A(q_1) - \Delta G°_1^A)) n(q_1) dq_1 \quad (7)$$

where $\delta(x) = 1$ for $x = 0$ and zero, otherwise, $n(q_1)$ is the Boltzmann fractional population associated to that particular nuclear configuration, and all the other magnitudes have their usual meaning or were defined above. The absorption

spectrum results from integration of eq 7 over all possible nuclear configurations

$$\epsilon(\nu) = \int_{-\infty}^{\infty} \frac{4\pi^2\nu}{3\hbar c n_t} |\mu_{12}^{A}(q_1)|^2 \, \delta(\nu - (\Delta G^{\circ A}_{2}(q_1) - \Delta G^{\circ A}_{1}))n(q_1)dq_1 \quad (8)$$

From the computational point of view, the spectrum can be calculated by setting discrete values for q_1 in an appropriate range and adding the differential contributions arising from every specific nuclear coordinate.

Trinuclear Systems (Three-State Model). We explore here two possible situations depicted in Scheme 4a and b. They represent different oxidation states of the molecules, but from the mathematical point of view, they can be described by the same Hamiltonian equation. The analysis follows essentially the same line as the two-state systems, except that the Hamiltonian equations expressed in the diabatic basis are replaced by

$$H = \begin{pmatrix} \lambda_1[(q_1 - 1/2)^2 + (q_2 - \sqrt{3}/2)^2] & H_{12} & H_{12} \\ H_{12} & \Delta G^\circ + \lambda_2[{q_1}^2 + {q_2}^2] & H_{23} \\ H_{12} & H_{23} & \Delta G^\circ + \lambda_2[(q_1 - 1)^2 + {q_2}^2] \end{pmatrix} \quad (9)$$

where q_1 and q_2 are dimensionless ET coordinates, λ_1 and λ_2 are related to the Marcus reorganization energies, and ΔG° measures the relative free energy of the diabatic states. Notice that depending on the situation ΔG° takes positive or negative values because the localized state (1) is lower in energy for the III−II−III case but becomes an excited state for the one-electron-reduced species.

The diabatic potential surfaces are still described as quadratic functions of the nuclear coordinates, but we introduced two different ET coordinates: an antisymmetric one (q_1), which transforms state 2 into state 3 as defined in Scheme 4, and a symmetric coordinate (q_2) related to a net-electron transfer between the bridging fragment and the terminal ones. This two-dimensional approach is in line with previous work,[4,7] and it is necessary to correctly describe the miminum nuclear degrees of freedom relating the three diabatic states.

The symmetry of the problem leaves only two off-diagonal matrix elements, H_{12} and H_{23}. The former connects states that result from a net one-electron transfer between neighbor fragments, and the latter represents the interaction between states that arise from an electron transfer between the terminal moieties. Diagonalization of the above Hamiltonian equation provides now three surfaces ($\Delta G^{\circ A}_{1}(q_1,q_2)$, $\Delta G^{\circ A}_{2}(q_1,q_2)$, and $\Delta G^{\circ A}_{3}(q_1,q_2)$ in increasing order of energy), and therefore two electronic transitions. The ET coordinate dependent energies of the adiabatic states and their compositions in terms of the diabatic basis set satisfy the relations

$$\psi_j^{A} = \sum_{i=1}^{3} C_{ij}(q_1)\psi_i^{D}(q_1) \quad (10)$$

$$\begin{pmatrix} \Delta G^{\circ A}_{1}(q_1,q_2) & 0 & 0 \\ 0 & \Delta G^{\circ A}_{2}(q_1,q_2) & 0 \\ 0 & 0 & \Delta G^{\circ A}_{3}(q_1,q_2) \end{pmatrix} = C(q_1,q_2)^{-1} \times H(q_1,q_2) \times C(q_1,q_2) \quad (11)$$

and using the same unitary transformation, we get the transition moment matrix in the adiabatic representation

$$\mu^{A}(q_1,q_2) = C(q_1,q_2)^{-1} \times \mu^{D} \times C(q_1,q_2) \quad (12)$$

where μ^{D} can be described by

$$\mu^{D} = \begin{pmatrix} 0 & 0 & 0 \\ 0 & -er & 0 \\ 0 & 0 & er \end{pmatrix} \quad (13)$$

The absorption profile from the lowest to the two excited adiabatic surfaces arises from integration of the differential absorption contributions over all the possible nuclear configurations of the ground state

$$\epsilon_{12}(\nu) = \int_{-\infty}^{\infty}\int_{-\infty}^{\infty} \frac{4\pi^2\nu}{3\hbar c n_t} |\mu_{12}^{A}(q_1,q_2)|^2 n(q_1,q_2)\delta(\nu - (\Delta G^{\circ A}_{2}(q_1,q_2) - \Delta G^{\circ A}_{1}(q_1,q_2)))dq_1dq_2 \quad (14)$$

$$\epsilon_{13}(\nu) = \int_{-\infty}^{\infty}\int_{-\infty}^{\infty} \frac{4\pi^2\nu}{3\hbar c n_t} |\mu_{13}^{A}(q_1,q_2)|^2 n(q_1,q_2)\delta(\nu - (\Delta G^{\circ A}_{3}(q_1,q_2) - \Delta G^{\circ A}_{1}(q_1,q_2)))dq_1dq_2 \quad (15)$$

Expressions 14 and 15 (or actually a discrete version over a rectangular grid) can be used to simulate the two components underlying the absorption profile of the reported trinuclear species.

Spectral Analysis. The above equations were employed to simulate the DACT absorption profiles and to fit these simulations to the experimental spectra. The prediction of the spectral band shape required a previous estimation of the dipole moments of the diabatic states involved in the analysis. In our case, we approximated those quantities by the geometric difference between the metal centers (5 *e*Å).[8] It is important to mention that Stark spectroscopy measurements in some mixed-valent cyanide-bridged dinuclear complexes[15,16] suggest that the effective one-electron-transfer distance, *r*, might be smaller than the geometric separation. However, the difference should remain small, provided that the degree of mixing between the fragments is not high.

The fitting procedure should provide the relevant physical parameters, ΔG°, the electronic coupling elements, and the reorganization energies. The number of fitting parameters is apparently high, but the physics of the problem imposes

(15) Vance, F. W.; Slone, R. V.; Stern, C. L.; Hupp, J. T. *Chem. Phys.* **2000**, *253*, 313−322.
(16) (a) Bublitz, G. U.; Laidlaw, W. M.; Denning, R. G.; Boxer, S. G. *J. Am. Chem. Soc.* **1998**, *120*, 6068−6075. (b) Vance, F. W.; Karki, L.; Reigle, J. K.; Hupp, J. T.; Ratner, M. A. *J. Phys. Chem. A* **1998**, *102*, 8320−8324.

Table 2. Absorption Maxima and Parameters Obtained from the Electronic Spectra for the Complexes Studied in This Work

	solvent	ν_{max}[a] (10^3 cm^{-1})	$\Delta G°$ (10^3 cm^{-1})	λ_1 (10^3 cm^{-1})	λ_2 (10^3cm^{-1})	H_{12} (10^3 cm^{-1})	$100C_{11}^2$ | $100C_{21}^2$ | $100C_{31}^2$ [c]
1	water	7.6	5.1	1.3	3.1	1.5	94.4 | 2.8 | 2.8
	methanol	10.2	7.5			1.3	97.2 | 1.4 | 1.4
	ethanol	10.8	8.1			1.2	97.8 | 1.1 | 1.1
	acetonitrile	13.1	10.4			1.1	98.7 | 0.64 | 0.64
	dimethylacetamide	14.3	11.6			1.0	99.1 | 0.45 | 0.45
2	water	6.9	4.5			1.4	94.4 | 2.8 | 2.8
	methanol	9.4	6.7			1.3	96.8 | 1.6 | 1.6
	ethanol	10.1	7.4			1.3	97.2 | 1.4 | 1.4
	acetonitrile	12.5	9.7			1.1	98.6 | 0.71 | 0.71
	dimethylacetamide	13.7	11.0			1.0	99.0 | 0.49 | 0.49
3	water	6.3	4.1			1.4	93.8 | 3.1 | 3.1
	methanol	8.7	6.0			1.4	95.8 | 2.1 | 2.1
	ethanol	9.4	6.7			1.3	96.8 | 1.6 | 1.6
	acetonitrile	12.0	9.3			1.1	98.5 | 0.75 | 0.75
	dimethylacetamide	13.1	10.4			1.0	98.9 | 0.53 | 0.53
1r	methanol	7.8	−1.6	7.1	9.9	1.4	97.3 | 0.1 | 2.6 0.1| 97.3| 2.6 2.4| 2.4| 95.2[d]
2r	methanol	7.2	−1.2			1.4	97.1 | 0.0 | 2.9 0.0 | 97.1 | 2.9 2.2 | 2.2 | 95.6[d]
3r	methanol	6.5	−0.4			1.5	96.1 | 0.0 | 3.9 0.0 | 96.1 | 3.9 2.1 | 2.1 | 95.8[d]
4	water	7.6[b]	5.0	1.3	3.2	1.4	95.7 | 4.3
	methanol	10.2[b]	7.5			1.3	97.9 | 2.1
	ethanol	10.9[b]	8.1			1.3	98.2 | 1.8
	acetonitrile	13.2[b]	10.6			1.1	99.2 | 0.83
	dimethylacetamide	14.4[b]	11.7			1.0	99.4 | 0.58

[a] Ref 8, except for compound **4**. [b] This work. [c] Computed coefficients at the equilibrium geometry for the ground-state normalized wave function $\psi_1^A = C_{11}\psi_1^D + C_{21}\psi_2^D + C_{31}\psi_3^D$, except for compound **4**, where $\psi_1^A = C_{11}\psi_1^D + C_{21}\psi_2^D$. [d] Compositions of the three minima observed in the ground-state PES.

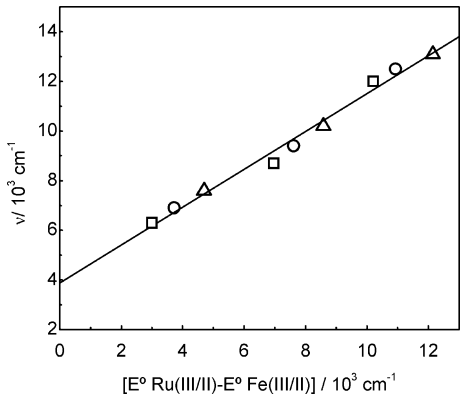

Figure 3. Correlation between the DACT energy and ΔE(redox) = $E°(Ru^{III/II}) - E°(Fe^{III/II})$ for species **1**−**3** in different solvents.

constraints on the possible values of these parameters and helps to avoid over-parametrization. For instance, the DACT bands in trinuclear **1** and model compound **4** have the same band shape in every solvent. However, they differ in the intensity, the CT bands of complex **1** being twice as intense as the same bands in complex **4** (Figure 2). If the parameters obtained from the fitting with a two-state model of the spectrum of complex **4** in a particular medium are used to simulate the spectrum of **1** in the same solvent with the three-state Hamiltonian with $H_{23} = 0$ and $H_{12} = H_{DA}$, the experimental spectrum is almost perfectly reproduced. The fact that the band profiles for both **1** and **4** can be well reproduced with the same set of parameters, which involves electronic coupling exclusively between neighbors, suggests that the direct interaction between the terminal fragments is negligible. This is compatible with previous qualitative observations in a related trinuclear system based on the $\{Pt^{IV}-(\mu-NC)-Fe^{II}\}$ unit.[17] For the remaining analysis, we assumed that H_{12} is the only relevant coupling element and set $H_{23} = 0$.

More constraints can be set on the physical parameters that describe the problem. Figure 3 shows a fairly linear correlation between the energy of the experimental DACT transition and the ΔE(redox) = $E°(Ru^{III/II}) - E°(Fe^{III/II})$ values for species **1**−**3** measured among the whole set of solvents. This result indicates that the reorganization energy associated with the electron-transfer process for this family of complexes can be considered essentially independent of the solvent and the identity of the L ligands.[18] The main contributions to λ are probably internal and arise from stretching vibrations involving the $\{Fe^{III}(\mu\text{-CN})Ru^{II}(\mu\text{-NC})\text{-}Fe^{III}\}$ backbone. The same is probably true for the Co^{III}-substituted species and for the one-electron-reduced systems. With this assessment in mind, we decided to keep λ_1 and λ_2 constant within each group of complexes (**1**−**3**, **1r**−**3r**, and **4**). The final optimized parameters obtained from the fitting

(17) Pfennig, B. W.; Lockard, J. V.; Cohen, J. L.; Watson, D. F.; Ho, D. M.; Bocarsly, A. B. *Inorg. Chem.* **1999**, *38*, 2941−2946.
(18) Lever, A. B. P.; Dodsworth, E. S. Electrochemistry, Charge-Transfer Spectroscopy, and Electronic Structure. In *Inorganic Electronic Structure and Spectroscopy*; Solomon, E. I., Lever, A. B. P., Eds.; J. Wiley & Sons: New York, 1999; Vol. II, pp 227−289.

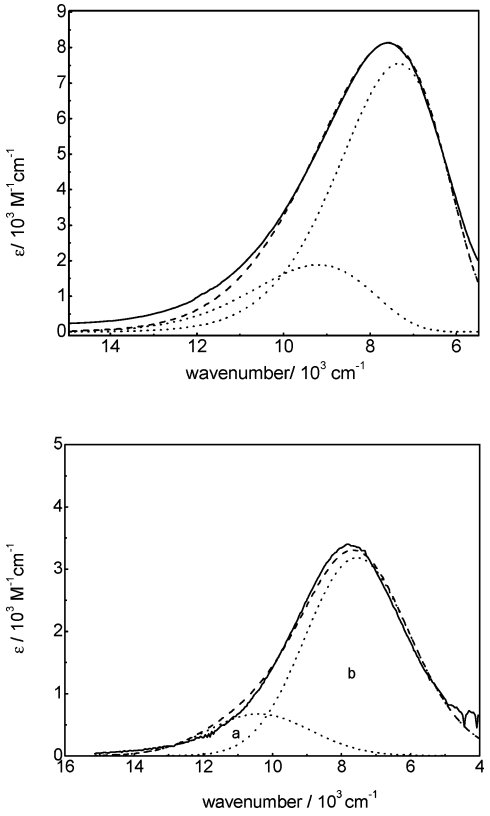

Figure 4. Experimental (solid line) and simulated (dotted line) DACT bands of complex **1** (top) and complex **1r** (bottom) in methanol. The dashed lines are the two components of the MMCT.

procedure are listed in Table 2. Typical simulated spectra deconvoluted into the two underlying absorption components are displayed in Figure 4, showing that the band shape of the experimental CT is well reproduced. This result applies to the whole set of simulated spectra (Supporting Information).

In compounds **1**−**3**, the values obtained for the diabatic free-energy difference, $\Delta G°$, vary smoothly with the acceptor capability of the solvent and reflect the stabilization of the excited states that have Fe^{II} character by specific interactions with the solvent.[8,12] The σ-donor capability of the pyridines coordinated to the central ruthenium controls the energy of the donor fragment. Table 2 reflects a decrease of $\Delta G°$ values as the basicity of L increases, which is consistent with our previous interpretation of the experimental trend.[8]

The values obtained for the electronic coupling parameter H_{12} are moderate and comparable to values reported in other cyanide-bridged dinuclear and polynuclear systems.[15,19] H_{12} appears to be roughly independent of the nature of the ligand L, but it depends on the acceptor capability of the solvent. This suggests that its value is mainly controlled by the electronic density distribution on the iron terminal fragments, which is modulated by cyanide−solvent specific interactions.

The combination of $\Delta G°$, H_{12}, and the reorganization energy yields a low degree of mixing of the diabatic excited states into the ground state. This results in a ground state that is essentially $\{Fe^{III}-Ru^{II}-Fe^{III}\}$ in character with small $\{Fe^{II}-Ru^{III}-Fe^{III}\}$ and $\{Fe^{III}-Ru^{III}-Fe^{II}\}$ (at most 3%) contributions. (Table 2). The highest mixing coefficients are achieved in solvents with high acceptor number[20] and correspond, as expected, to the combination of low diabatic energies and high electronic-coupling values. Inspection of the potential energy surfaces reveals that for complexes **1**−**3** there are no crossings between the diabatic ground-state surfaces and the excited ones because of the larger value of λ_2 with respect to λ_1. The adiabatic ground-state surface has therefore only one minimum, which implies that the hypothetical electronic isomers $\{Fe^{II}-Ru^{III}-Fe^{III}\}$ are not stable species in these systems.

The analysis of the DACT transitions in compounds **1r**−**3r** is depicted in Figure 5. A weak mainly $Fe^{II} \rightarrow Fe^{III}$ in character CT absorption shows up at the high-energy side of the DACT band and a more intense $Ru^{II} \rightarrow Fe^{III}$ CT appears at the low-energy side. The spectroscopic data obtained for the two deconvoluted components of the DACT band of compounds **1r**−**3r** are listed in Table 3. As expected, the energy of the $Fe^{II} \rightarrow Fe^{III}$ component remains independent of the identity of the ligand L, while the second one is red shifted when the basicity of L is increased. For these species, the values of H_{12} (Table 2) are similar to those found for compounds **1**−**3**, but the differences between the energies of the diabatic ground and excited states become substantially smaller. This observation can be traced back to the presence of an extra electron in the $\{Fe^{II}(CN)_6\}^{4-}$ moiety of **1r**−**3r** that increases the electronic density of the donor fragment if compared to the **1**−**3** case.

The PES for the adiabatic ground state is different than that in **1**−**3** (Figure 6). The picture changes because of the doubly degenerate diabatic ground state and the existence of intersections between the diabatic ground and excited surfaces. The ground-state PES presents three local minima corresponding to the three possible electronic isomers. Figure 6, which represents the situation in methanol, displays the minimum energy pathways and the activation barrier, $\Delta G^{\ddagger}$, for the thermal-activated electron transfer between the minima, calculated by means of standard methodology.[21] There are mainly two possible mechanisms for the electron transfer between the terminal iron moieties in these cyanide-bridged trinuclear compounds. One is the superexchange path, where the bridge, in this case, the Ru^{II} fragment, mediates the electronic mixing between the donor and the

(19) (a) Watzky, M. A.; Macatangay, A. V.; VanCamp, R. A.; Mazzetto, S. E.; Song, X. Q.; Endicott, J. F.; Buranda, T. *J. Phys. Chem. A* **1997**, *101*, 8441−8459. (b) Scandola, F.; Argazzi, R.; Bignozzi, C. A.; Chiorboli, C.; Indelli, M. T.; Rampi, M. A. *Coord. Chem. Rev.* **1993**, *125*, 283−292. (c) Forlano, P.; Baraldo, L. M.; Olabe, J. A.; Dellavedova, C. O. *Inorg. Chim. Acta* **1994**, *223*, 37−42. (d) Endicott, J. E.; Chen, Y. J.; Xie, P. H. *Coord. Chem. Rev.* **2005**, *249*, 343−373. (e) Macatangay, A. V.; Endicott, J. F. *Inorg. Chem.* **2000**, *39*, 437−446. (f) Oshio, H.; Onodera, H.; Ito, T. *Chem.—Eur. J.* **2003**, *9*, 3946−3950. (g) Pfennig, B. W.; Fritchman, V. A.; Hayman, K. A. *Inorg. Chem.* **2001**, *40*, 255−263. (h) Rogez, G.; Marvilliers, A.; Sarr, P.; Parsons, S.; Teat, S. J.; Ricard, L.; Mallah, T. *Chem. Commun.* **2002**, 1460−1461. (i) Rogez, G.; Riviere, E.; Mallah, T. *C. R. Chim.* **2003**, *6*, 283−290. (j) Vogler, A.; Kisslinger, J. *J. Am. Chem. Soc.* **1982**, *104*, 2311−2312.
(20) Gutmann, V. *Electrochim. Acta* **1976**, *21*, 661−670.
(21) (a) Henkelman, G.; Uberuaga, B. P.; Jonsson, H. *J. Chem. Phys.* **2000**, *113*, 9901−9904. (b) Henkelman, G.; Jonsson, H. *J. Chem. Phys.* **2000**, *113*, 9978−9985.

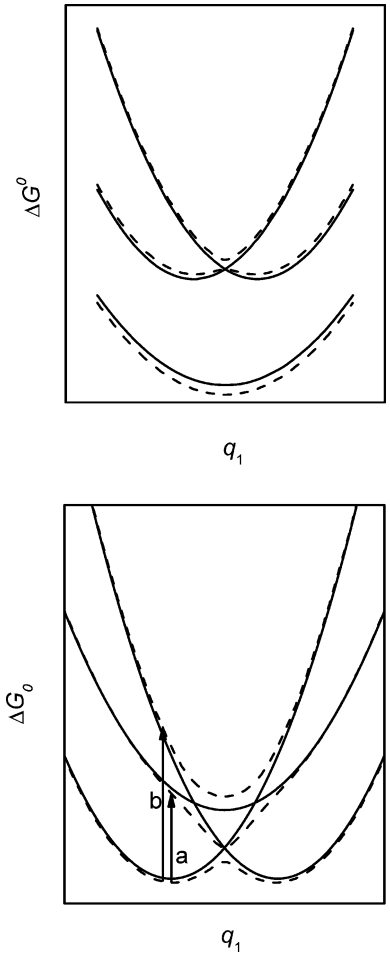

Figure 5. 2-D slice at $q_2 = 0$ of the diabatic (solid line) and adiabatic (dotted line) potential energy surfaces for compounds **1** (top) and **1r** (bottom); a and b identify the two $Fe^{II} \rightarrow Fe^{III}$ and $Ru^{II} \rightarrow Fe^{III}$ DACT, respectively.

Table 3. Absorption Maxima and Intensity of the Deconvoluted $Ru^{II} \rightarrow Fe^{III}$ and $Fe^{II} \rightarrow Fe^{III}$ DACT Bands in Compounds **1r**−**3r**

	CT $Ru^{II} \rightarrow Fe^{III}$		CT $Fe^{II} \rightarrow Fe^{III}$	
	ν_{max} (10^3 cm^{-1})	μ^2 (eÅ)^2	ν_{max} (10^3 cm^{-1})	μ^2 (eÅ)^2
1r	7.6	0.64	10.3	0.098
2r	7.3	0.81	10.3	0.088
3r	6.7	1.2	10.2	0.104

acceptor.[22] The other one is the hopping mechanism, where the bridge effectively participates in the ET process by means of the electronic isomer $\{Fe^{II}-Ru^{III}-Fe^{II}\}$.[23] The surfaces displayed in Figure 6 predict that both mechanisms have to contribute sizably to the ET process in compound **1r**. However, in the case of compounds **2r** and **3r**, the lower-energy separation between the ground and excited diabatic states leaves no saddle points in the region between the $\{Fe^{III}-Ru^{II}-Fe^{II}\}$ and $\{Fe^{II}-Ru^{II}-Fe^{III}\}$ stable configurations. This suggests that the electron transfer should proceed solely by a hopping pathway. It seems that for this family

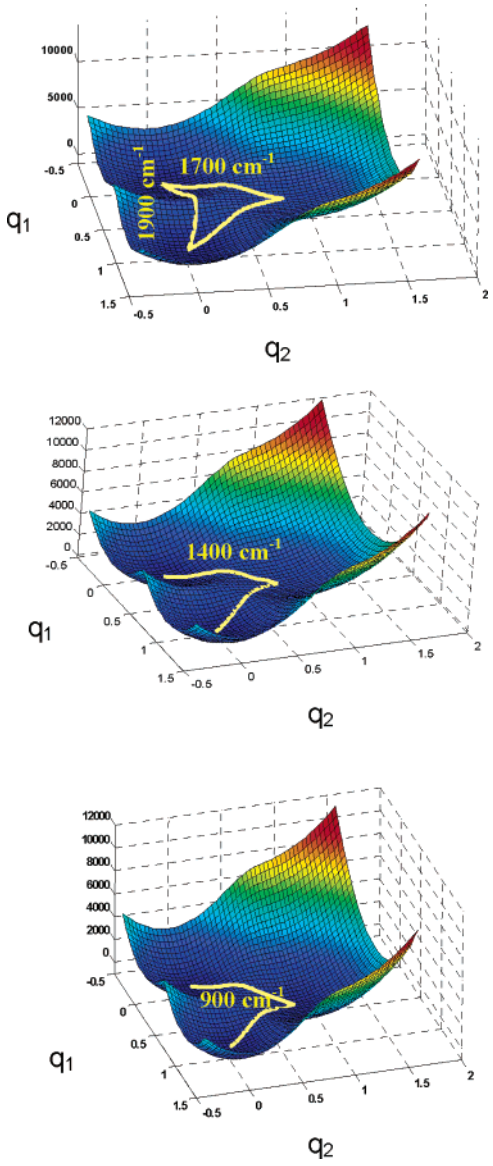

Figure 6. Ground-state potential energy surfaces of the one-electron-reduced complexes, **1r**−**3r**, showing the minimum energy electron-transfer trajectories between the minima. The values correspond to the activation barriers.

of trinuclear compounds the type of mechanism of ET can be tuned by a suitable choice of the ligand L.

Conclusions

Despite approximations, the three-state model is able to reproduce the experimental band shape of the DACT absorption of a family of binuclear and trinuclear cyanide-bridged compounds in different solvents, providing a numerical estimate of the degree of electronic interaction between the fragments. One of the most interesting results obtained from our analysis is the invariance of the reorganization energy, λ, for changes in the solvent or the substituents on the pyridinic rings. This suggests that the vibrational modes coupled with the electron-transfer remain the same in all the measured systems. Raman studies should be useful to explore this issue.

For the reduced **1r**−**3r** species, the model predicts a ground-state potential energy surface with three minima that

(22) (a) Bixon, M.; Jortner, J. *Electron Transfer—From Isolated Molecules To Biomolecules*; J. Wiley & Sons: New York, 1999; Vol. 106. (b) Jortner, J.; Bixon, M.; Langenbacher, T.; Michel-Beyerle, M. E. *Proc. Natl. Acad. Sci. U.S.A.* **1998**, *95*, 12759−12765.

(23) Berlin, Y. A.; Burin, A. L.; Ratner, M. A. *Chem. Phys.* **2002**, *275*, 61−74.

correspond roughly to the intuitive description where the odd electron is placed alternatively on each metal center. The thermal barriers connecting the electronic isomers are small, and the actual mechanism could vary in different compounds.

The calculated values of H_{12} are significant, but they are not high enough to promote a delocalized ground state. If we assume that the reorganization energies could remain comparable for other substituted pyridines, a delocalized ground state can be expected for an H_{12} of $\sim$3000 cm^{-1}. Such a value might be reached by employing an electron-richer ruthenium complex. Alternatively, a better electronic interaction can be achieved by replacing iron with a metal of the second or the third transition period. We are currently exploring these ideas.

Acknowledgment. The authors thank the University of Buenos Aires, the Consejo Nacional de Investigaciones Científicas y Técnicas (CONICET), and Fundación Antorchas for economic funding. We are also thankful to Johnson Matthey for a generous loan of $RuCl_3$. L.M.B. and L.D.S. are members of the scientific staff of CONICET; M.B.R. is a fellow of the same institution, and P. A. is a fellow from the University of Buenos Aires.

Supporting Information Available: Electronic spectra in the NIR region for species **1**−**3**, **4**, and **1r**−**3r** in different solvents, including the deconvolution into the underlying components as described in the text. This material is available free of charge via the Internet at http://pubs.acs.org.

IC061202K